Title	Molecular dynamics simulations of vacancy diffusion in chromium(III) oxide, hematite, magnetite and chromite
Author(s)	Vaari, Jukka
Citation	Solid State Ionics. Elsevier. Vol. 270 (2015), Pages 10 - 17
Date	2015
URL	http://dx.doi.org/10.1016/j.ssi.2014.11.027
Rights	Post-print version of the article. This article may be downloaded for personal use only.

Molecular dynamics simulations of vacancy diffusion in chromium(III) oxide, hematite, magnetite and chromite

Jukka Vaari

VTT Technical Research Centre of Finland
Kemistintie 3, P.O. Box 1000, FI-02044 VTT, Finland
+358-40-5233692, jukka.vaari@vtt.fi

Abstract

Mass transport in bulk α-Cr_2O_3, α-Fe_2O_3, Fe_3O_4 and $FeCr_2O_4$ has been studied by means of classical molecular dynamics (MD) simulations. Point defects were assumed to be responsible for ionic diffusion. The focus of this study were vacancies both in the cation and anion lattice (Schottky defects). The Buckingham potential was used to describe the interactions between ions. Defect concentrations in the 10^{-4} to 10^{-3} range were studied in the temperature range 1300 K – 2000 K. Diffusion coefficients were calculated from mean square displacements. Activation energies for migration were determined from Arrhenius plots.

Keywords

Molecular dynamics, mass transport, migration energy, Schottky defects

Introduction

Mass transport properties of metal oxides have attracted much experimental, theoretical and computational attention due to the importance of a surface oxide layer in determining the lifetime of metallic components in a wide range of applications. The oxides investigated in this work are typically formed on the surface of a low-alloy steel during exposure to high-temperature oxidative environments, as exemplified by Figure 1 [1]. This shows the outward diffusion of iron to form the outer oxide consisting of magnetite and hematite layers, and inward diffusion of oxygen together with enrichment of Cr to form the mixed hematite-chromite inner layer. The aim in this work is to provide insight, using atomistic simulation methods, on the details of the diffusion processes involved.

Despite the prevalence of these oxides, we have found surprisingly little work done using atomistic simulation methods related to the mass transport properties. Catlow et al [2] determined lattice and electronic defect formation and migration energies for α-Cr_2O_3 and α-Fe_2O_3, based on a Mott-Littleton approach. Later Atkinson et al [3] extended the approach to include lattice defects induced by impurities. Direct MD simulations on bulk diffusion for these materials seem to be missing. However, MD simulations have been reported on the ordering of α-Cr_2O_3(0001) surface [4,5].

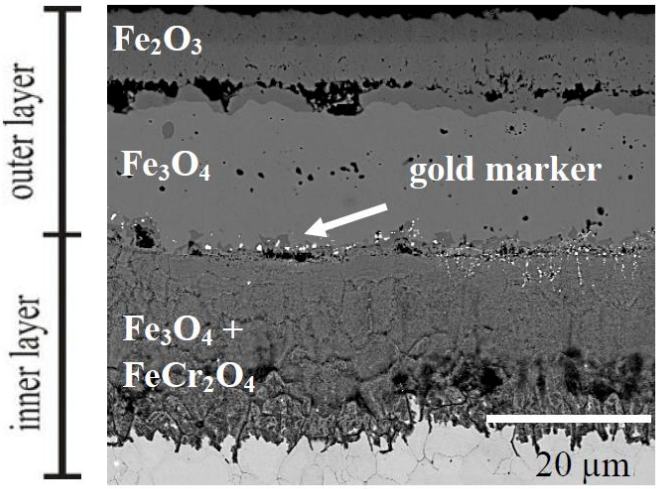

Figure 1. Oxide scale on a low alloy steel (grade X60) after exposure at 550 °C to laboratory air for 72 h.

One complicating factor related to MD work is the complex defect chemistry of these oxides, yielding a large number of possible initial configurations for the simulations. The defect chemistry is affected both by impurities as well as the sample preparation procedure. Holt and Kofstad [6] report elevated levels of Mg and Al impurities in their Cr_2O_3 samples due to extended exposure to the materials in the conductivity measuring instruments. According to Atkinson et al [3], small divalent substitutional cations (such as Mg) in a Cr_2O_3 lattice have solution energies of the order of 2 eV, significantly less than the energies of intrinsic defect formation. This implies that real Cr_2O_3 samples should be regarded as doped semiconductors with the charge carrier concentration dictated by the impurity concentration.

The focus in this study is diffusion due to point defects. However even the nature of the dominant point defect type in the oxides of this study is not always fully agreed on. For example, Su and Simkovich [7] present a comprehensive analysis on the point defect structure of Cr_2O_3 fully starting out from the assumption that the point defects are in the cation lattice. Young et al [8] acknowledge the possibility of defects in the oxygen lattice to explain the observed p-type conductivity in their Cr_2O_3 samples, but go on to conclude that Cr lattice defects are a more plausible explanation. Holt and Kofstad [9], in a study of Mg-doped Cr_2O_3, discuss the possibility of defects in the oxygen lattice, a conclusion supported by the calculations by Atkinson et al [3].

We will entirely concentrate on Schottky-type point defects. Energetics and mechanisms of defect formation will not be studied. Instead, pre-defined defect concentrations will be used. The defect concentrations used in the simulations are in the 10^{-4} to 10^{-3} range in order to ensure minimal interaction between individual defects and to avoid defect clustering. Simulations are conducted in temperature range 1300 K – 2000 K in order to determine the activation energy of migration.

Computational details

The atomic interactions in this work were described by a Buckingham potential in combination with a Coulomb term:

$$V_{ij}(r_{ij}) = A_{ij}\exp\left(-\frac{r_{ij}}{\rho_{ij}}\right) - \frac{C_{ij}}{r_{ij}^6} + \frac{q_i q_j}{r_{ij}}$$

The parameters used in the simulations are shown in Table 1. Two different parameters sets applicable to α-Cr_2O_3 and α-Fe_2O_3 were used. Pairwise interactions were explicitly calculated up to a distance of 15 Å.

Long-range Coulombic interactions were computed by the Ewald method. Polarization effects were not accounted for. Only Coulombic interaction was assumed between cations due to the small radius of these ions. All ions were assumed to adopt their formal charges.

For α-Cr_2O_3 and α-Fe_2O_3, a supercell of 20 x 20 x 10 hexagonal unit cells with periodic boundary conditions was used in the simulations for a total of 120000 atoms. For Fe_3O_4 and $FeCr_2O_4$, a supercell of 15 x 15 x 15 cubical unit cells (189000 atoms) with periodic boundary conditions was used. In the case of Fe_3O_4 reverse spinel, one Fe^{3+} cation was placed in the tetrahedral site, and the remaining Fe^{3+} cation and the Fe^{2+} cation were randomly distributed in the octahedral holes. Schottky defects were generated by randomly deleting atoms from both cation and anion lattices to maintain charge neutrality. The integration of Newton's equations was performed by the Verlet algorithm. A time step of 1.0 fs was used. All simulations were conducted in the NPT ensemble. Simulations were typically run up to 400 ps (α-Cr_2O_3 and α-Fe_2O_3) of 600 ps (Fe_3O_4 and $FeCr_2O_4$) of real time.

The diffusion of ions was measured by recording the Mean Square Displacement (MSD) for ion type i as a function of time, and computing the diffusion constant from the slope of the MSD(t) curve according to

$$\left\langle r_i^2(t)\right\rangle = \frac{1}{N}\sum_N \left[r_i(t) - r_i(0)\right]^2 = 6Dt$$

To obtain the slope, a line was fitted to the MSD(t) curve from 200 ps to 400 ps for α-Cr_2O_3 and α-Fe_2O_3, and from 200 ps to 600 ps for Fe_3O_4 and $FeCr_2O_4$.

The MD simulations were performed using LAMMPS software [10].

Table 1. Buckingham potential parameterizations used in this work.

Oxide	Interaction	A (eV)	r (Å)	C (eV·Å^6)	Reference
Cr_2O_3, set1	$Cr^{3+} - O^{2-}$	1734.1	0.301	0	[11]
	$O^{2-} - O^{2-}$	22764	0.149	27.88	[12]
Cr_2O_3, set2	$Cr^{3+} - O^{2-}$	1204.18	0.3165	0	[13]
	$O^{2-} - O^{2-}$	9547.96	0.2192	32	[13]
Fe_2O_3, set1	$Fe^{3+} - O^{2-}$	1102.4	0.3299	0	[11]
	$O^{2-} - O^{2-}$	22764	0.149	27.88	[12]
Fe_2O_3, set2	$Fe^{3+} - O^{2-}$	1414.6	0.3128	0	[13]
	$O^{2-} - O^{2-}$	9547.96	0.2192	32	[13]
Fe_3O_4	$Fe^{3+} - O^{2-}$	1414.6	0.3128	0	[13]
	$Fe^{2+} - O^{2-}$	649.1	0.3399	0	[11]
	$O^{2-} - O^{2-}$	9547.96	0.2192	32	[13]
$FeCr_2O_4$	$Cr^{3+} - O^{2-}$	1204.18	0.3165	0	[13]
	$Fe^{2+} - O^{2-}$	649.1	0.3399	0	[11]
	$O^{2-} - O^{2-}$	9547.96	0.2192	32	[13]

Results

Simulations for α-Cr_2O_3 and α-Fe_2O_3 were performed for defect concentrations of $8.3\cdot10^{-5}$, $2.0\cdot10^{-4}$, $\cdot4.2\cdot10^{-4}$, and $8.3\cdot10^{-4}$ and for temperatures from 1300 K to 2000 K at 100 K intervals. The defects were created at 300 K, followed by a 10 ps heating time from 300 K to the target temperature. Figure 2 presents typical MSD(t) curves from the simulations for α-Cr_2O_3. The time zero in the figure has been set to the point in time when the simulation has reached the target temperature. This explains the initial non-zero MSD values which are slightly different for the two parameter sets. The data contains considerable noise due to the low defect concentration, limiting the accuracy of determining the slope of the MSD(t) curve especially at lower temperatures. The main difference between the parameter sets is that for set 1, oxygen

appears to be the mobile ion, while chromium shows essentially no diffusion. For set 2, both ions are mobile. Since both chromium and oxygen are experimentally known to be mobile species [6,14], parameter set 2 is believed to better represent mass diffusion in α-Cr_2O_3.

It can be observed from Figure 2 that for parameter set 2, the initial 10 ps heating period is not sufficient to equilibrate the system. The shape of the MSD curves is curved up to about 200 ps, after which a linear trend continues. This is the reason for determining diffusion coefficients from the MSD data after 200 ps.

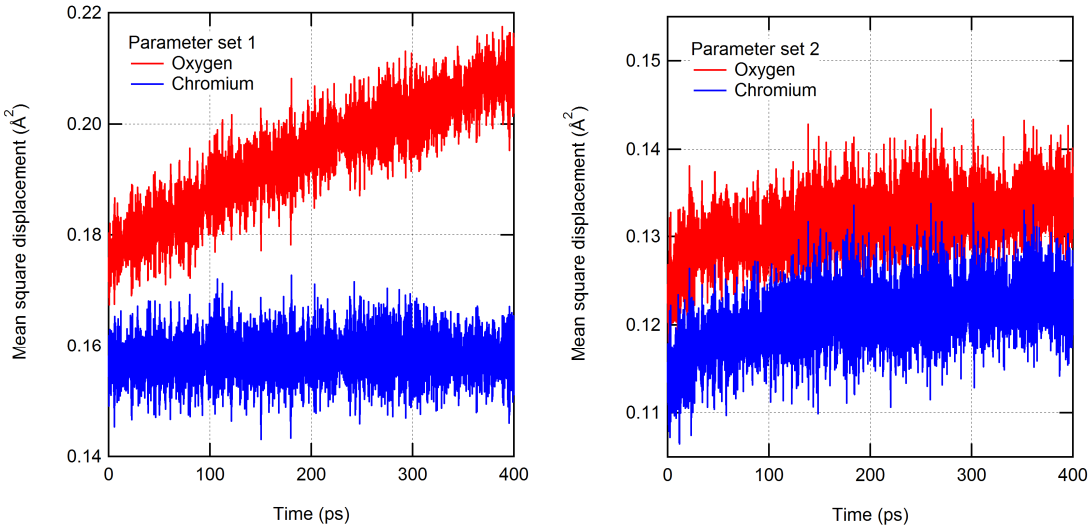

Figure 2. Mean square displacement of oxygen and chromium ions in α-Cr_2O_3 for a Schottky defect concentration of $8.3 \cdot 10^{-4}$ at a temperature of 1500 K. Left: Parameter set 1. Right: Parameter set 2.

The diffusion coefficients determined from the simulations for α-Cr_2O_3 at a Schottky defect concentration of $8.3 \cdot 10^{-4}$ are presented in Figure 3. Chromium data for parameter set 1 is not presented, as the MSD curves for chromium showed no slope that could have been determined reliably even at a temperature of 2000 K. The data (especially for Cr) contains scatter, which can be partly understood by the noise in the raw MSD data due to the low defect concentration, as exemplified by Figure 2. Other sources of scatter include the initial defect configuration and the initial velocity distribution. To investigate the effect of the two latter sources, simulations with parameter set 2 were repeated by varying both the defect configuration and the initial velocity distribution. For T=1600 K, a total of five simulations were conducted. The results suggest that the initial configuration has an important effect on the determination of the diffusion coefficient. For oxygen, the migration activation energy and the values of the diffusion coefficient agree fairly well between the two parameterizations of the interaction potential.

The diffusion coefficients determined from the simulations for α-Fe_2O_3 at a Schottky defect concentration of $8.3 \cdot 10^{-4}$ are presented in Figure 4. In this case it can be noted that both parameter sets predict mobility for both the anion and the cation, in agreement with the experimental findings by Amami et al [15]. As with α-Cr_2O_3, the scatter in the cation data is larger than for anion. No repeated simulations were carried out for α-Fe_2O_3; however for parameter set 2, additional data was obtained for temperatures of 1350K, 1450K and 1550 K. For Fe, the two parameter sets predict practically the same activation energy for migration, but the values of Fe diffusion coefficient for parameter set 2 are two orders of magnitude larger. For oxygen there are significant differences both in the values of the activation energy and the diffusion coefficient.

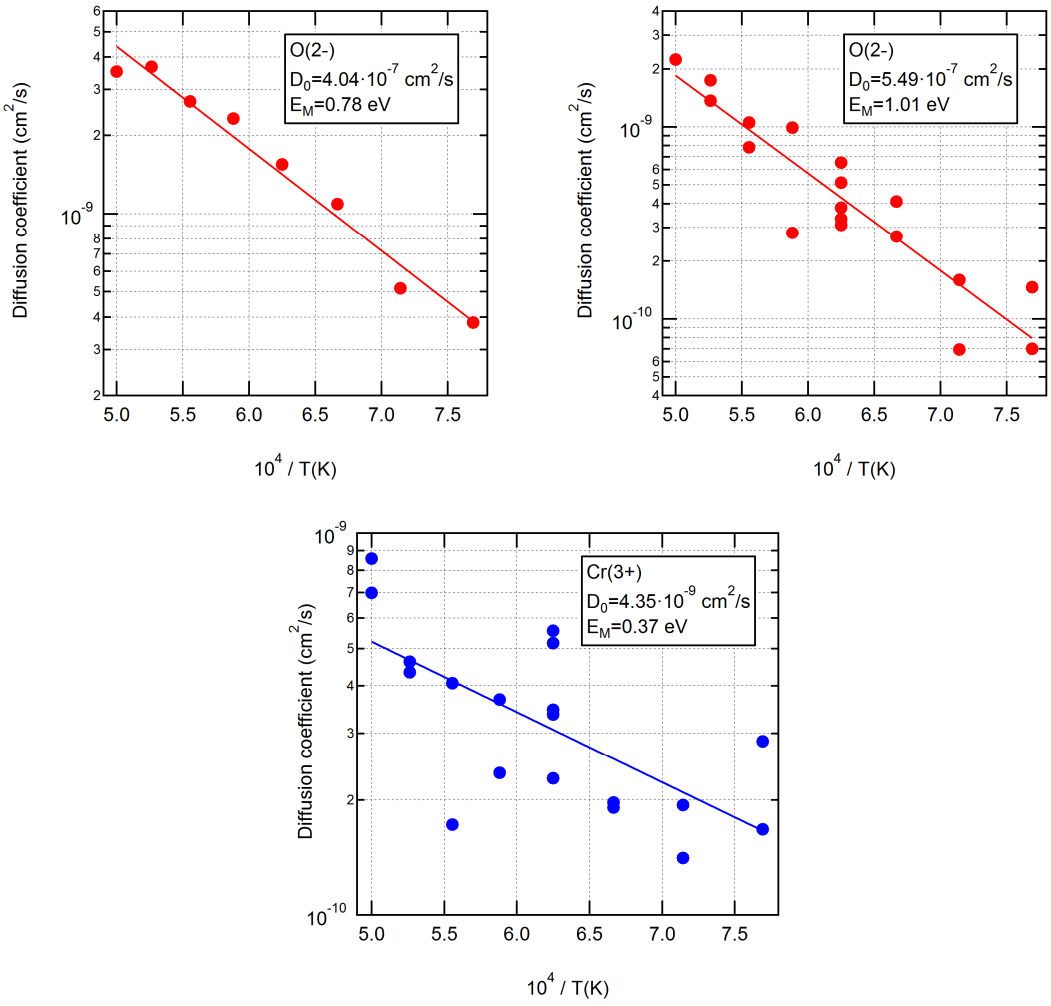

Figure 3. Diffusion coefficients (markers), Arrhenius fits (lines) and Arrhenius parameters (annotations) for O and Cr diffusion in α-Cr_2O_3 for parameter sets 1 and 2 at a Schottky defect concentration of $8.3 \cdot 10^{-4}$. Top left: D_O for parameter set 1. Top right: D_O for parameter set 2. Bottom: D_{Cr} for parameter set 2.

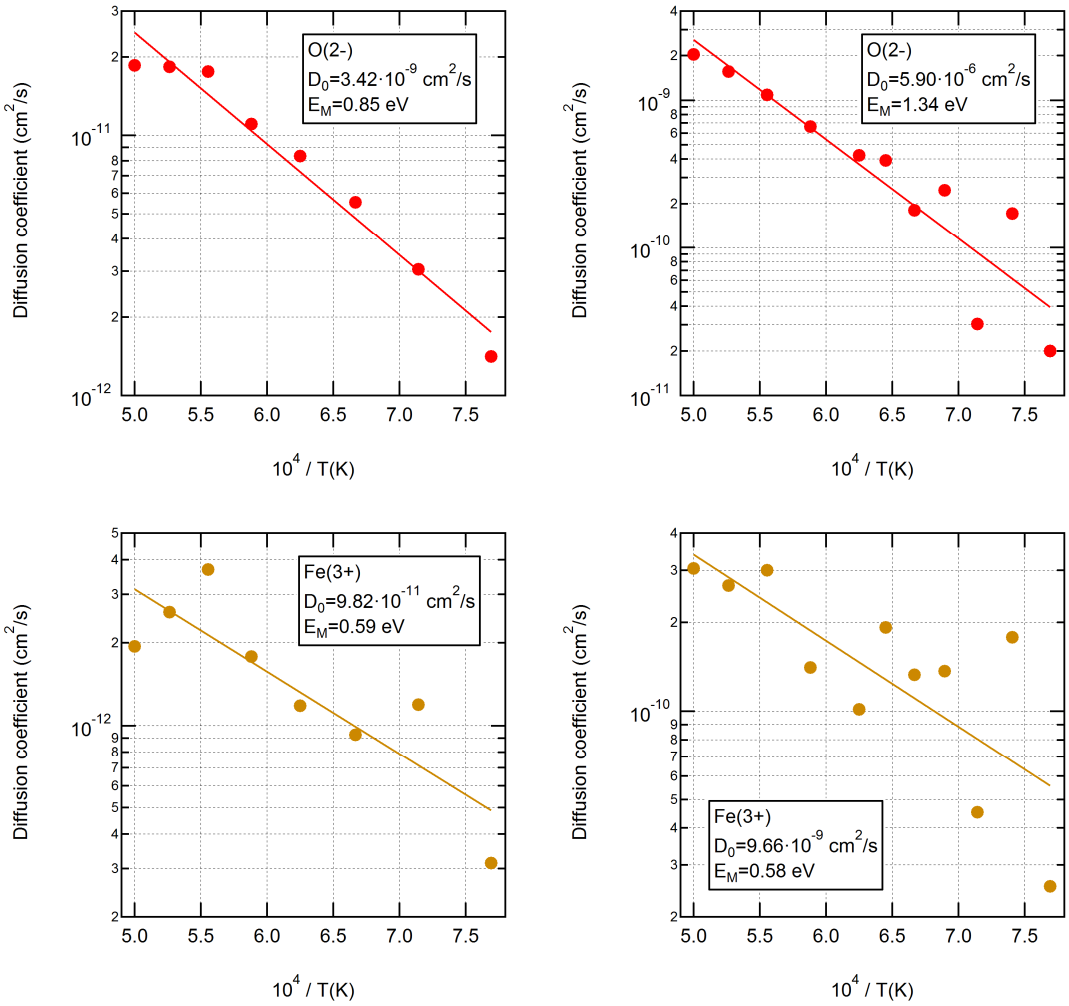

Figure 4. Diffusion coefficients (markers), Arrhenius fits (lines) and Arrhenius parameters (annotations) for O and Fe diffusion in α-Fe_2O_3 for parameter sets 1 and 2 at a Schottky defect concentration of $8.3 \cdot 10^{-4}$. Top left: D_O for parameter set 1. Top right: D_O for parameter set 2. Bottom left: D_{Fe} for parameter set 1. Bottom right: D_{Fe} for parameter set 2.

The Fe^{2+} diffusion coefficients determined from the simulations for Fe_3O_4 at a Schottky defect concentration of $6.7 \cdot 10^{-4}$ are presented in Figure 5. The migration activation energy for Fe^{2+} in Fe_3O_4 is similar to Fe^{3+} in Fe_2O_3, but the value of the diffusion coefficient for Fe^{2+} in Fe_3O_4 is an order of magnitude larger than for Fe^{3+} in Fe_2O_3 (parameter set 2). The parameterization used for the interaction potential did not predict detectable diffusion for the Fe^{3+} cation or oxygen. Experimentally, the majority defects in Fe_3O_4 are believed to be either cation vacancies or interstitials, depending on oxygen partial pressure [16,17]. Diffusion of oxygen in Fe_3O_4 has been studied by Millot and Niu [18] who determined the oxygen defects to be either free oxygen vacancies (low oxygen pressures) or anion-cation vacancy pairs (high oxygen pressures). The latter defect type was not included in this study. However for oxygen vacancies, the MD results are at qualitative variance with experiments.

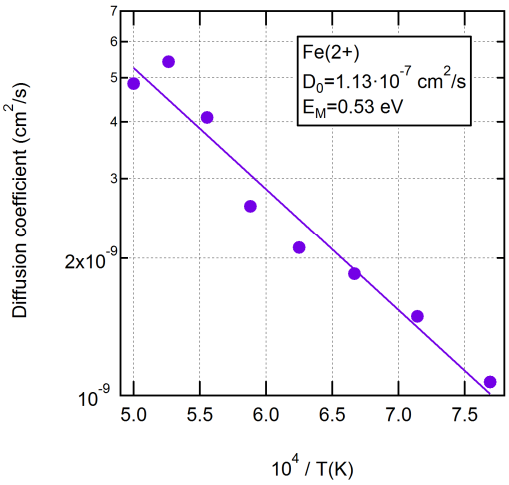

Figure 5. Diffusion coefficients (markers), Arrhenius fit (line) and Arrhenius parameters (annotation) for Fe^{2+} diffusion in Fe_3O_4 at a Schottky defect concentration of $6.7 \cdot 10^{-4}$.

The diffusion coefficients determined from the simulations for $FeCr_2O_4$ at a Schottky defect concentration of $6.7 \cdot 10^{-4}$ are presented in Figure 6. All ions are mobile, but Fe^{2+} has the largest diffusion coefficient and the smallest activation energy for migration. The Fe^{2+} data also shows the largest scatter, which is attributed to the fact that only one ion out of seven is Fe^{2+} so the statistics is inherently worse compared to other ions. Here it is interesting to note the study by Nagata et al [19] on $FeCr_2O_4$ spinel formation in a FeO/Cr_2O_3 interface. They attribute the spinel formation to Fe^{2+} diffusion through spinel and subsequent reaction at spinel/Cr_2O_3 interface. The bulk diffusion coefficients reported by Gilewicz-Wolter et al [20] for Fe and Cr in $FeCr_2O_4$ are close to each other.

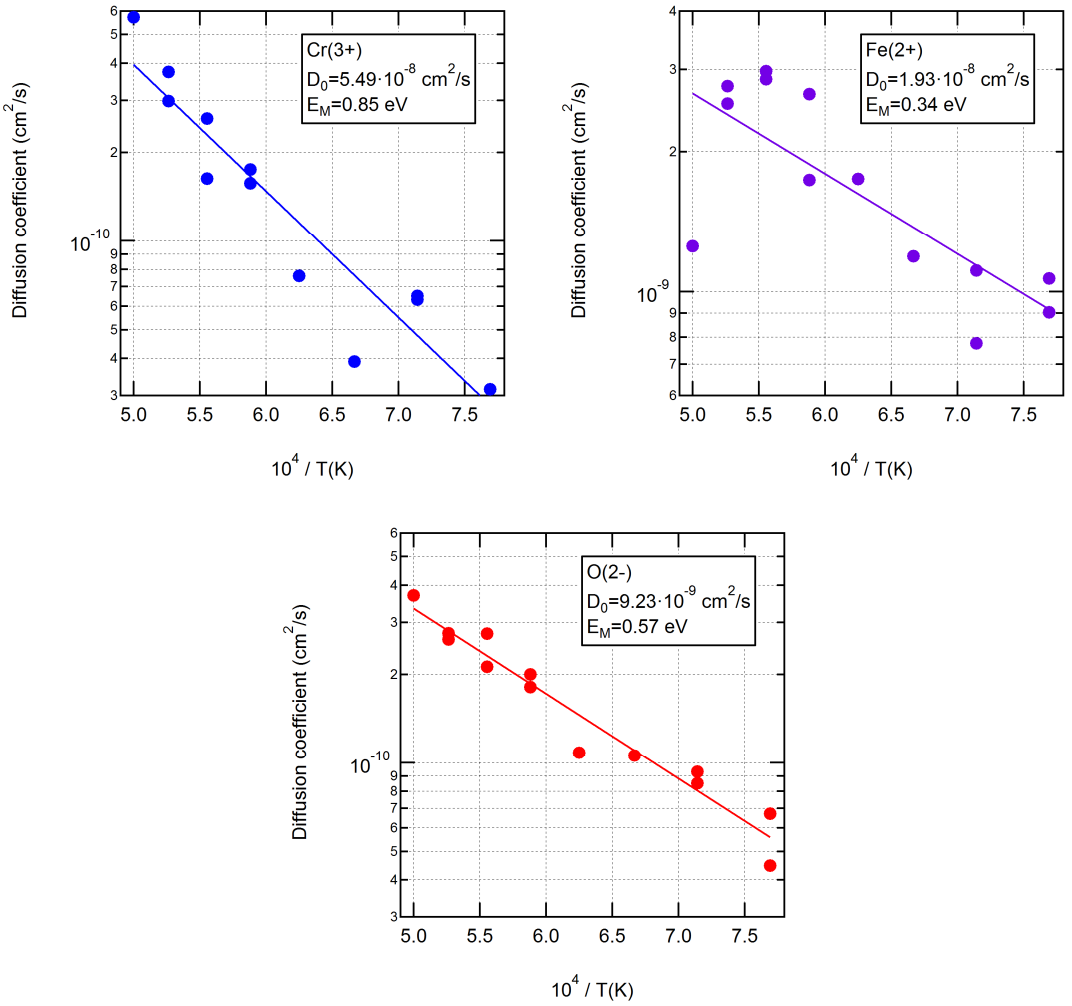

Figure 6. Diffusion coefficients (markers), Arrhenius fits (lines) and Arrhenius parameters (annotations) for diffusion in $FeCr_2O_4$ at a Schottky defect concentration of $6.7 \cdot 10^{-4}$.

The dependence of the oxygen diffusion coefficient on the defect concentration for α-Cr_2O_3 is presented in Figure 7. It can be observed that the dependence seems to be close to linear for the three lower defect concentrations studied, but a deviation from linearity occurs when going to the highest defect concentration especially for temperatures between 1300 K and 1700 K. This suggest that at a defect concentration of $8.3 \cdot 10^{-4}$ the defects can no longer be regarded as completely isolated from each other. In particular, the possibility of two defects being initially close to each other increases, which gives more freedom for the lattice to deform and allow atoms to diffuse. Marrocchelli et al [21] studied defect-induced lattice expansion around oxygen vacancies in several fluorite-structured oxides, and from their molecular dynamics simulations they concluded that vacancies start to significantly interact with each other above a critical concentration of $2.5 \cdot 10^{-4}$.

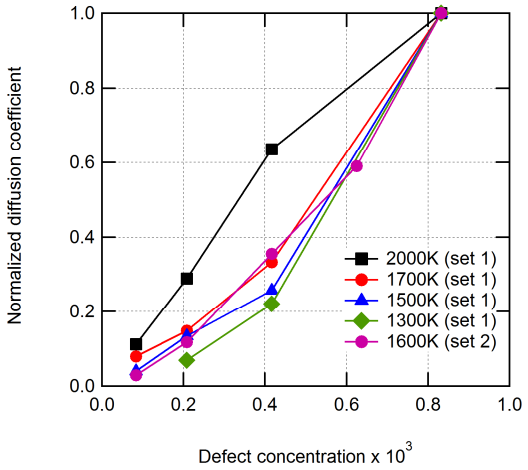

Figure 7. Normalized oxygen diffusion coefficients as a function of Schottky defect concentration for α-Cr_2O_3. Solid markers correspond to parameter set 1, and open markers to parameter set 2.

Discussion

The diffusion coefficient can be expressed in the form

$$D = D_0 \exp\left(-\frac{E_A}{kT}\right) = D_0 \exp\left(-\frac{E_F + E_M}{kT}\right)$$

where E_A is the overall activation energy for diffusion and which contains contributions due to defect formation (E_F) and migration (E_M). The results of this study are directly concerned with E_M, since mechanisms and energetics of defect formation is not modelled. The implications of the E_M values for E_F are however discussed below.

Only few experimental studies were found in literature that concerned the activation energy for migration for the defect types and materials of this study. The activation energies for electronic and ionic diffusion in Cr_2O_3 scales grown on Ni-20%Cr alloy were measured by Liu et al [22] using asymmetry polarization technique. Whereas pure electronic conductivity was observed above 700 °C, mixed electronic and ionic conductivity was observed below 700 °C. The activation energies for electronic and ionic conductivities were 0.6 eV and 0.3 eV, respectively. The analysis in [22] assumes that chromium interstitials dominate the ionic conduction. However the activation energy of 0.3 eV for ionic conduction is close to the activation energy of 0.37 eV found in Figure 4 for Cr vacancy diffusion. Betova et al [23] determined kinetic and transport parameters for the inner oxide layer on AISI 316 L(NG) stainless steel in temperature range of 150 – 300 °C using the mixed-conduction model [24], and found activation energies of 0.45 eV and 0.51 eV for chromium and iron diffusion, respectively

Horita et al [25] used an isotope tracer technique to study oxygen diffusion in the oxide scales formed on Fe-Cr –based ferritic stainless steels. The oxide scales consisted of a Fe-Mn spinel on top of a layer described as 'Cr-rich spinel or Cr_2O_3'. These authors found an activation energy of 1.4 eV for oxygen diffusion, somewhat larger than the value of 1.01 eV found for α-Cr_2O_3 in Figure 3 for parameter set 2 and significantly larger than the value of 0.57 eV found for $FeCr_2O_4$ in Figure 6.

Temperature dependent diffusion coefficients in Cr_2O_3 have been reported by several authors. Kofstad and Lillerud [14] present a compilation of data from Hagel and Seybolt [26], Hagel [27], Lindner and Åkerström [28] and Walters and Grace [29]. These data can be fitted with the following expressions:

$$D_{Cr} = 4.3 \cdot 10^3 \exp\left(-415\left(kJ/mol\right)/RT\right) \quad cm^2/s$$ (sintered samples)

$$D_{Cr} = 0.167 \exp\left(-255\left(kJ/mol\right)/RT\right) \quad cm^2/s$$ (hot-pressed samples)

$$D_O = 15.9 \exp\left(-422\left(kJ/mol\right)/RT\right) \quad cm^2/s$$

The difference in the D_{Cr} values between the two sample preparation methods illustrates the difficulties in obtaining consistent experimental data for diffusion coefficients. The same conclusion was later drawn by Tsai et al [30] who noted that the experimental diffusion coefficients presented by various authors can vary by orders of magnitude.

Amami et al [15] measured temperature dependent bulk diffusion coefficients in Fe_2O_3 natural single crystals in the temperature range 890 to 1227 ºC. Their data can be fitted as follows:

$$D_{Fe} = 9.2 \cdot 10^{10} a\left(O_2\right)^{-0.56} \exp\left(-578\left(kJ/mol\right)/RT\right) \quad cm^2/s$$

$$D_O = 2.7 \cdot 10^8 a\left(O_2\right)^{-0.26} \exp\left(-542\left(kJ/mol\right)/RT\right) \quad cm^2/s$$

The activation energy for iron is close to 510 kJ/mol determined by Sabioni et al [31] for their Fe_2O_3 single crystal samples above 1200 K. It can be noted that the activation energies for diffusion are higher in in Fe_2O_3 single crystals as compared to Cr_2O_3 samples prepared from powders.

Besides morphology, an issue connected to sample preparation are impurities whose role has been pointed out in several studies [3,6-9]. The computational work by Atkinson et al [3] provides important insight into the energetics of defect formation due to impurities in α-Al_2O_3, α-Cr_2O_3 and α-Fe_2O_3. In particular, they find that aliovalent dopants with a small ionic radius in these materials (such as Mg^{2+} or Ti^{4+}) may have solution energies as low as about 2 eV, which are significantly lower than the formation energy of intrinsic defects. In addition, such doping will drive up the concentration of point defects through charge compensating reactions.

Atkinson et al [3] also report intrinsic defect energies for Schottky, anion Frenkel and cation Frenkel defects. For Schottky defects in α-Cr_2O_3 this is 5.59 eV, which is in excess of an earlier estimate of 4.22 eV by Catlow et al [2]. Considering now the activation energies appearing in the expression for the diffusion coefficients for Cr in α-Cr_2O_3, and subtracting the migration activation energy for Cr obtained in this work (0.37 eV), we arrive at defect formation energies of 3.93 eV for sintered samples, and 2.27 eV for hot-pressed samples. Similarly from the oxygen data we get a defect formation energy of 3.36 eV. These are substantially below the intrinsic defect energies, suggesting that impurities are dominating the defect structure in these materials.

The situation is somewhat different for natural Fe_2O_3 single crystals. The activation energies for diffusion are close to the intrinsic Schottky defect energy of 5.82 eV [3]. The impurity levels in the natural single crystals were typically below 50 ppm for aliovalent impurities. Amami et al [15] report an activation energy of 9.44 eV for Fe diffusion along grain boundaries, attributing the high value to segregation of the impurities to grain boundaries or dislocation walls.

Given the estimates on the defect formation energies it is instructive to examine the defect concentrations that these suggest, and to compare these to the ones used in this study. Generally, the point defect concentration in a bulk crystal is given by

$$n/N = \exp\left(-E_F/RT\right)$$

where n is the number of defects, N the total number of lattice sites (or structural formula units), and E_F is the formation energy of an isolated defect (where we assume n<<N). Figure 8 presents the equilibrium

defect concentration as a function of temperature for selected values of E_F. When considering defect concentrations in real materials, it is important to understand the temperature history of the samples. For example, Holt and Kofstad [6] prepared their Cr_2O_3 samples by first cold-pressing high-purity Cr_2O_3 powder followed by either sintering for one hour at 1783 K or by hot-pressing at 1673 K for one hour. Whenever diffusion measurements are done at lower temperatures, it can be expected that the defect structure of the samples corresponds to the high-temperature conditions during sample preparation, because diffusion processes in these materials are slow. Salomonsen et al [32] suggest that in Cr_2O_3, the defect structure is "frozen in" below 1300K, but is equilibrated with the surroundings at higher temperature. Figure 8 suggests that even for the lowest defect formation energies around 2 eV, the point defect concentration remains below the ppm range for practical temperatures.

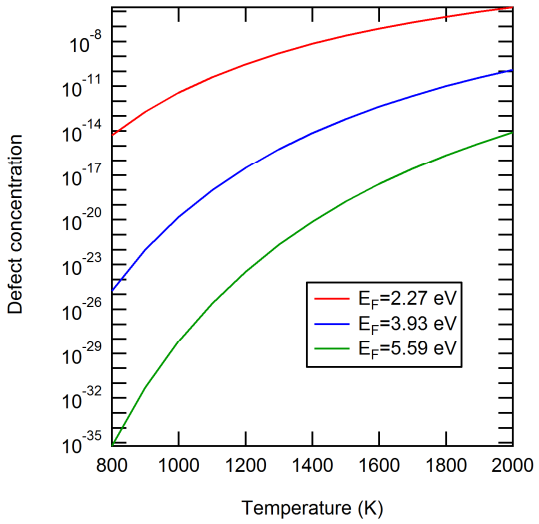

Figure 8. Equilibrium concentration of point defects as a function of temperature for selected defect formation energies.

The defect concentrations used in this work were 2-4 orders of magnitude higher than the highest concentrations suggested by Figure 8. As explained in conjunction with Figure 2, this was necessary to detect enough diffusion events within the computational time available. On the other hand, it was desired that the defects were isolated from each other, which was probably not the case with the highest defect concentrations used (see Figure 7). This means that a direct computational measurement of diffusion events in a crystal with realistic point defect concentrations is computationally challenging, if not impossible, for defects with a high formation energy and at low temperatures.

Assuming however that for isolated defects the overall diffusion coefficient is linearly proportional to the point defect concentration, it is possible to extrapolate the results to lower defect concentrations. To exemplify this, we employ the data by Tsai et al [30] who determined Cr and O bulk and grain boundary diffusion constants at 1073 K and 1173 K from Cr_2O_3 scales grown by oxidation on $Ni_{70}Cr_{30}$ alloy. The experimental data is shown in Figure 9 together with linear fits to the Arrhenius plots of Figure 3 (parameter set 2) which are extended down to the experimental temperatures. It is stressed that the slope in the lines is entirely due to the activation energy for migration. There is no change in the defect concentration as a function of temperature.

It is seen that extrapolation of the MD data for a defect concentration of $8.3 \cdot 10^{-4}$ (the highest defect concentration involved in this study) passes close to the experimental grain boundary diffusion coefficients. Decreasing the defect concentration to $2.5 \cdot 10^{-6}$ makes the MD data pass close to the apparent diffusion coefficient data. In order to make the MD data pass close to the bulk diffusion data, the defect concentration needs to be decreased well below the ppm range, which is in line with the defect concentrations in Figure 8.

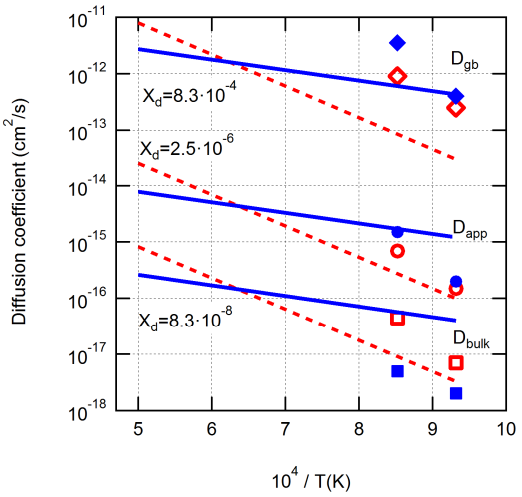

Figure 9**.** Extrapolation of calculated Cr and O diffusion coefficients in α-Cr_2O_3 to lower temperatures and defect concentrations for parameter set 2 and for three different defect concentrations. The lines are the extended linear Arrhenius fits to Cr (solid lines) and O (dotted lines) data of Figure 3. The markers are the experimental data by Tsai et al (1996) for Cr (solid) and O (open) bulk diffusion (squares), grain boundary diffusion (diamonds) and apparent (spheres) diffusion coefficients.

Only a limited amount of information is available on the defect concentrations in the oxides relevant to this study. Young et al [8] employed Seebeck measurements to obtain defect concentrations. In this case, the measured thermoelectric power (ε) relates to the concentration of charge carriers (n) through $\varepsilon=(k/e)\ln(N/n)$ where k is the Boltzmann constant and N is the density of states, which is taken equal to the number of cation sites. For p-type Cr_2O_3 at temperatures below 1300 K Young et al find a thermoelectric power of 750 µV/K corresponding to an electron hole concentration of $2\cdot10^{-4}$ per cation site. Young et al then assume that chromium vacancies are present in the p-type material. Since one vacancy in a triply charged lattice corresponds to three holes, they arrive at a defect concentration of $6.7\cdot10^{-5}$. Su and Simkovich [7] also applied Seebeck measurements to determine the point defect structure in pure and doped Cr_2O_3. At 1400 K temperature they found a defect concentration of approximately $1\cdot10^{-5}$. These defect concentrations correspond to typical impurity levels in the low ppm range. In addition, the Seebeck measurements do not differentiate between charge carriers in the bulk and on grain boundaries. The defect concentration of $2.5\cdot10^{-6}$ used in Figure 9 to approximately reproduce the apparent diffusion coefficients is slightly below the values suggested by experiments.

Conclusions

Classical molecular dynamics simulations were used to gain insight into the relationship between the defect structure and mass transport properties of α-Cr_2O_3, α-Fe_2O_3, Fe_3O_4 and $FeCr_2O_4$. The focus in this study were Schottky defects, i.e. transport through lattice vacancies. Energetics and mechanisms of defect formation were not studied. Instead, pre-defined defect concentrations were used. Accordingly, the study yielded activation energies for migration in the case of vacancy diffusion.

Direct molecular dynamics simulations were conducted. Thermal noise and infrequency of transition events reduced the detection limit for diffusion coefficient to around 10^{-12} cm^2/s. This required the use of defect concentrations in the 10^{-4} to 10^{-3} range and temperatures in the 1300 K – 2000 K range. These defect concentrations were higher than those expected in bulk material. Extrapolation of diffusion coefficients to lower defect concentrations was done by assuming that diffusion constants are linearly proportional to the defect concentration. Extrapolation of diffusion coefficients to lower temperatures was done through an Arrhenius plot.

Activation energies for migration were determined from the Arrhenius plots. For cations, these ranged between 0.37 eV and 0.91 eV, while for oxygen these ranged from 0.57 eV to 1.34 eV. For vacancy diffu-

sion in α-Cr_2O_3 and α-Fe_2O_3, cations were clearly more mobile than oxygen. For $FeCr_2O_4$, the mobility of the ions behaved as $Fe^{2+} > O^{2-} > Cr^{3+}$. For Fe_3O_4, only Fe^{2+} exhibited mobility that was detectable in the simulations.

For α-Cr_2O_3 and α-Fe_2O_3, we showed that the results are sensitive to the Buckingham potential parameterization used. Especially for α-Cr_2O_3, one parameter set resulted in oxygen mobility only, while another parameter set, both chromium and oxygen were mobile.

References

[1] Baxter, D. and Heikinheimo, L. (eds.) (2005). Opticorr Guide Book. Optimization of in-service performance of boiler steels by modelling high-temperature corrosion. VTT Research Notes 2309. VTT, Espoo, Finland. http://www.vtt.fi/publications (accessed 24.11.2014)

[2] Catlow, C.R.A., Corish, J., Hennessy, J. and Mackrodt, W.C. (1988). Atomistic simulations of defect structures and ion transport in α-Fe_2O_3 and α-Cr_2O_3. Journal of the American Ceramic Society vol. 71 pp. 42.49.

[3] Atkinson, K.J.W, Grimes, R.W., Levy, M.R., Coull, Z.L. and English, T. (2003). Accommodation of impurities in α-Al_2O_3, α-Cr_2O_3 and α-Fe_2O_3. Journal of the European Ceramic Society vol. 23 pp. 3059-3070.

[4] San Miguel, M.A., Álvarez, L.J., Sanz, J.F. and Odriozola, J.A. (1999). Cr_2O_3(0001) oxygen-terminating surface. A molecular dynamics study. Journal of Molecular Structure (Theochem) vol. 463 pp. 185-190.

[5] Sun, J., Stirner, T. and Matthews, A. (2007). Molecular dynamics studies of the (0001) α-Al_2O_3 and α-Cr_2O_3 surfaces. Surface Science vol. 601 pp.1358-1364.

[6] Holt, A. and Kofstad, P. (1994). Electrical conductivity and defect structure of Cr_2O_3. Part 1. High temperatures (> ~1000 °C). Solid State Ionics vol. 69 pp. 127-136.

[7] Su, M.Y. and Simkovich, G. (1987). Point defect structure of Cr_2O_3. Technical Report No. TR 87-008. The Pennsylvania State University, Applied Research Laboratory.

[8] Young, E.W.A., Gerretsen, J.H. and de Wit, J.H.W. 1987. The Oxygen Partial Pressure Dependence of the Defect Structure of Chromium(III) Oxide. Journal of the Electrochemical Society: Solid-State Science and Technology vol. 134 pp. 2257-2260.

[9] Holt, A. and Kofstad, P. (1997). Electrical conductivity and defect structure of Mg-doped Cr_2O_3. Solid State Ionics vol. 100 pp. 201-209.

[10] Plimpton, S.J. (1995). Fast Parallel Algorithms for Short-Range Molecular Dynamics. Journal of Computational Physics vol. 117 pp. 1-19.

[11] Lewis, G.V. and Catlow, C.R.A. (1985). Potential models for ionic oxides. Journal of Physics C: Solid State Physics vol. 18 pp. 1149-1161.

[12] Catlow, C.R.A. (1977). Point Defect and Electronic properties of Uranium Dioxide. Proceedings of the Royal Society A vol. 353 pp. 533-561.

[13] Minervini, L., Zacate, M.O. and Grimes, R.W. (1999). Defect cluster formation in M_2O_3-doped CeO_2. Solid State Ionics vol. 116 pp. 339-349.

[14] Kofstad, P. and Lillerud, K.P. (1980). On high temperature oxidation of chromium. Part 2. Properties of Cr_2O_3 and the oxidation mechanism of chromium. Journal of Electrochemical Society: Solid-state Science and Technology vol 127 pp 2410-2419.

[15] Amami, B., Addou, M., Millot, F., Sabioni, A. and Monty, C. (1999). Self-diffusion in α-Fe_2O_3 natural single crystals. Ionics, vol. 5 pp. 358-370.

[16] Dorris, S. and Martin, M. (1990). Magnetite (Fe_3O_4) in an oxygen potential gradient: chemical diffusion, tracer diffusion and phase boundary reaction. Berichte der Bunsengesellschaft für physikalische Chemie vol. 94 pp. 721-726.

[17] Aggarwal, S., Töpfer, J., Tsai, T.-S. and Dieckmann, R. (1997). Point defects and transport properties in binary, tertiary and non-stoichiometric oxides. Solid State Ionics vol. 101-130, pp. 321-331.

[18] Millot, F. and Niu, Y. (1997). Diffusion of O^{18} in Fe_3O_4. An experimental approach to study the behaviour of minority defects in oxides. Journal of Physics and Chemistry of Solids vol. 58 pp. 63-72.

[19] Nagata, K., Nishiwagi, R., Nakamura, Y. and Maruyama, T. (1991). Kinetic mechanisms of $MgCr_2O_4$ and $FeCr_2O_4$ spinels from their metal oxides. Solid State Ionics vol. 49 pp. 161-166.

[20] Gilewicz-Wolter, J., Zurek, Z., Dudala, J., Lis, J., Homa, M. and Wolter, M. (2006). Diffusion rates of 51Cr, 54Mn and 59Fe in $MnCr_2O_4$ and $FeCr_2O_4$ spinels. Advances in Science and Technology vol. 46 pp. 27-31.

[21] Marrocchelli, D., Bishop, S.R. and Kilner, J. (2013), Chemical expansion and its dependence on the host cation radius. Journal of Materials Chemistry A vol. 1 pp. 7673-7680.

[22] Liu, H., Stack, M.M. and Lyon, S.B. (1998). Reactive element effects on the ionic transport processes in Cr_2O_3 scales. Solid State Ionics vol. 109 pp. 247-257.

[23] Betova, I., Bojinov, M., Kinnunen, P. and Saario, T. (2007). Mixed Conduction Model for Oxide films - quantitative procedure for determination of kinetic parameters for individual species. VTT Research Report No VTT-R-04098-07. http://www.vtt.fi/publications (accessed 24.11.2014)

[24] Beverskog, B., Bojinov, M., Englund, A., Kinnunen, P., Laitinen, T., Mäkelä, K., Saario, T. and Sirkiä, P. (2002). A mixed-conduction model for oxide films on Fe, Cr and Fe-Cr alloys in high-temperature aqueous electrolytes. Part 1. Comparison of the electrochemical behaviour at room temperature and at 200 °C. Corrosion Science vol. 44 pp. 1901-1921.

[25] Horita, T., Kishimoto, H., Yamaji, K., Xiong, Y., Brito, M.E., Yokokawa, H., Baba, Y., Ogasawara, K., Kameda, H. and Matsuzaki, Y. (2008). Diffusion of oxygen in the scales of Fe-Cr alloy interconnects and oxide coating layer for solid oxide fuel cells. Solid State Ionics vol. 179 pp. 2216-2221.

[26] Hagel, W.C. and Seybolt, A.U. (1961). Cation diffusion in Cr_2O_3. Journal of Electrochemical Society: Solid-state Science and Technology vol. 108 pp 1146-1152.

[27] Hagel, W.C. (1965). Anion diffusion in α-Cr_2O_3. Journal of the American Ceramic Society vol. 48 pp. 70-75.

[28] Lindner, R. and Åkerstrøm, Å. (1956). Selbstdiffusion und Reaktion in Oxyd- und Spinellsystemen. Zeitschrift für Physikalische Chemie vol. 6 pp. 162-177.

[29] Walters, L.C. and Grace, R.E. (1965). Self diffusion of ^{51}Cr in single crystals of Cr_2O_3. Journal of Applied Physics vol. 36 p. 2331.

[30] Tsai, S.C., Huntz, A.M. and Dolin, C. (1996). Growth mechanism of Cr_2O_3 scales: oxygen and chromium diffusion, oxidation kinetics and effect of yttrium. Materials Science and Engineering vol. A212, pp. 6-13.

[31] Sabioni, A.C.S., Daniel, A.M.J.M., Macedo, W.A.A., Martins, M.D., Huntz, A.M., Jomard, F. and Persiano, A.I.C. (2005). First study of iron self-diffusion in Fe_2O_3 single crystals by SIMS. Defect and Diffusion Forum vol. 237-240 pp. 277-281.

[32] Salomonsen, G., Norman, N., Lønsjø, O. and Finstad, T.G. (1989). Kinetics and mechanism of oxide formation on Cr thin films. Journal of Physics: Condensed Matter vol. 1 pp. 7843-7850.